What is the Valence of Mn in Ga_{1−x}Mn_{x}N?

Ryky Nelson, Tom Berlijn, Juana Moreno, Mark Jarrell, and Wei Ku (□□)

Phys. Rev. Lett. **115**, 197203 — Published 4 November 2015

DOI: 10.1103/PhysRevLett.115.197203

What is the valence of Mn in $Ga_{1-x}Mn_xN$?

Ryky Nelson,[1,2] Tom Berlijn,[3] Juana Moreno,[1,2] Mark Jarrell,[1,2] and Wei Ku(顧威)[4,5]

[1]*Department of Physics & Astronomy, Louisiana State University, Baton Rouge, LA 70803*
[2]*Center for Computation & Technology, Louisiana State University, Baton Rouge, LA 70803*
[3]*Center for Nanophase Materials Sciences and Computer Science and Mathematics Division, Oak Ridge National Laboratory, Oak Ridge, TN 37831*
[4]*Condensed Matter Physics and Materials Science Department, Brookhaven National Laboratory, Upton, New York 11973*
[5]*Physics Department, State University of New York, Stony Brook, New York 11790*

(Dated: October 22, 2015)

We investigate the current debate on the Mn valence in $Ga_{1-x}Mn_xN$, a diluted magnetic semiconductor (DMS) with potential high Curie temperature. From a first-principles Wannier-function analysis, we find unambiguously the Mn valence to be close to 2+ (d^5), but in a mixed spin configuration with average magnetic moments of $4\mu_B$. By integrating out high-energy degrees of freedom differently, we further derive for the first time from first-principles two low-energy pictures that reflect the intrinsic dual nature of the doped holes in the DMS: 1) an effective d^4 picture ideal for local physics, and 2) an effective d^5 picture suitable for extended properties. In the latter, our results further reveal a few novel physical effects, and pave the way for future realistic studies of magnetism. Our study not only resolves one of the outstanding key controversies of the field, but also exemplifies the general need for multiple effective descriptions to account for the rich low-energy physics in many-body systems in general.

PACS numbers: 75.50.Pp, 75.30.Et, 71.15.Mb

Diluted magnetic semiconductors (DMS) have attracted great interest because of their potential applications in spintronic technology [1] such as nonvolatile memory [2, 3], spin-generating solar cells [4, 5], electrical spin injection [6], spin-LED (light-emitting diode) [7], and electrically or optically controlled ferromagnets [8]. Among the DMS materials, $Ga_{1-x}Mn_xN$ is of particular interest and increasingly studied. One of the motivations is that the blue LED [9–11] technology is based on the host compound GaN. $Ga_{1-x}Mn_xN$ also might be instrumental toward the realization of efficient spintronic devices as Dietl *et al.* [12] predicted its Curie temperature (T_c) to be above room temperature; a feature which is obviously required in order to be technologically advantageous. However, until now this prediction remains far from being fulfilled as various experiments lead to controversial conclusions concerning the ferromagnetism in $Ga_{1-x}Mn_xN$. Chen *et al.* [13] detected superparamagnetism in their nano-cluster $Ga_{1-x}Mn_xN$ sample, while Zając *et al.* [14] and Granville *et al.* [15] report antiferromagnetic coupling between Mn ions in their sample. Interestingly, Dhar *et al.* [16] in their investigation observe a Heisenberg spin-glass with a transition temperature around 4.5 K. Observations of the desired ferromagnetic ordering on the other hand have also been reported, albeit with fiercely varying T_c's; some [17, 18] find low T_c's between 10K and 25K, while others [19, 20] report ferromagnetism around room temperature or higher [21].

One factor considered to be instrumental for the magnetic order and the coupling mechanism in DMS is the valence state of Mn [22–24]. There is no doubt that in addition to a local moment, a (Ga,Mn) substitution injects a hole into the system, but the question is: where is this hole located? If the hole resides mostly in the N-valence bands and is likely delocalized, resulting in a Mn valence of 2+(d^5). In this case, similar to $Ga_{1-x}Mn_xAs$ systems [12, 25], the microscopic mechanism is described by pictures of Zener's kinetic-exchange type [26], in which the coupling between local moments is mediated by valence-band itinerant carriers. This mechanism has been examined experimentally for $Ga_{1-x}Mn_xAs$ [6, 27–30]. If, on the other hand, the hole resides mostly in Mn ions, the Mn valence is 3+(d^4), and the magnetic coupling would be better described by a double-exchange mechanism [31, 32] mediated by impurity levels [24, 33].

Despite its widely accepted importance, the Mn valence state in $Ga_{1-x}Mn_xN$ is still controversial. Early experimental [34–36] and density functional theory (DFT) studies [37–42] demonstrated a partially-filled impurity band formed deeply in the band gap with a significant Mn d-character, suggesting a Mn^{3+} (d^4) configuration different from the Mn^{2+} (d^5) one in $Ga_{1-x}Mn_xAs$ [43]. Later, both X-ray absorption spectroscopy (XAS) studies [44–46] and optical absorption analysis [47, 48] also concluded a Mn valence state of 3+ (d^4). However, other XAS studies [49–51] demonstrate that Mn is predominantly Mn^{2+} (d^5). A similar conclusion was also reached by electron spin resonance [14] and magnetic measurements [15]. Clearly, a resolution of the uncertainty about the Mn valence state is imperative for further progress in the understanding and engineering of the $Ga_{1-x}Mn_xN$ DMS.

In this Letter, we investigate the controversial Mn valence state in $Ga_{1-x}Mn_xN$. Our first-principles Wannier-

functions based analysis [52] covering the high-energy Hilbert space demonstrates unambiguously that the Mn valence is close to 2+ (d^5) but with a mixed spin configuration that gives average magnetic moments of $4\mu_B$ (*not* $5\mu_B$). Interestingly, at the more relevant lower-energy scale, due to the proximity of N s and p energy levels to the Mn d level, the dual nature of the doped hole can be realized. Defining Wannier orbitals (WOs) in a narrower energy range, we show the feasibility of both the effective d^4 and d^5 descriptions, which are convenient to describe different physical aspects of $Ga_{1-x}Mn_xN$. The resulting effective d^4 picture offers the simplest description of the local magnetic moment and the Jahn-Teller distortion while the effective d^5 picture is most suitable for long-range magnetic order. Moreover, our first-principles result reveals several strong physical effects absent in previous studies. Our study not only resolves one of the outstanding key puzzles in the field of DMS, but also highlights the generic need for multiple effective descriptions in describing the rich low-energy physics in interacting systems in general.

We start by performing first-principles DFT calculations in a zincblende supercell of 64 atoms ($Ga_{31}MnN_{32}$) within the full-potential linearized augmented-plane-wave method [53]. The LDA+U approximation [54] is applied to Mn atoms with $U = 4$ eV and $J = 0.8$ eV. We then construct WOs [52] in three different ways to effectively integrate out various degrees of freedoms, to analyze the electronic structure at different energy scales, and to illustrate the relevant physical effects. As will become clear below, the use of WOs is crucial in the analysis, for example in counting the charges.

First, to address the question on the valence state of Mn we look into the high-energy properties by analyzing the resulting density of states with N-sp^3, Ga-sp^3, and Mn-d symmetries covering the energy range of $[-18.0, 9.0]$ eV. Fig. 1(a) shows partially filled impurity bands lying deep in the band gap similarly to previous DFT analyses [24, 37–41]. Particularly, Fig. 1 (b) shows that the Mn-t_{2g} impurity levels are strongly hybridized with the surrounding N-sp^3 orbitals, such that the total weight in the N-orbital slightly exceeds that of the Mn. Integrating the DOS up to the Fermi energy, we find the Mn occupation to be 5.0, corresponding to the Mn valence of 2+ (d^5). This result is quite different from the value of 4.59 presented in a previous DFT study [37], but the distinction is easily understandable from the fact that counting charges within an artificially chosen muffin-tin around the Mn ion would necessarily miss the interstitial contributions. Our WOs, on the other hand, span the entire Hilbert space up to 9 eV and leaves no unaccountable charges.

However, this seemingly clean Mn^{2+} charge distribution contributes to a total spin of only 4.0 μ_B (*not* 5 μ_B). Therefore, it should not (and cannot) be understood simply from the pure ionic d^5 configuration. Indeed, Fig.

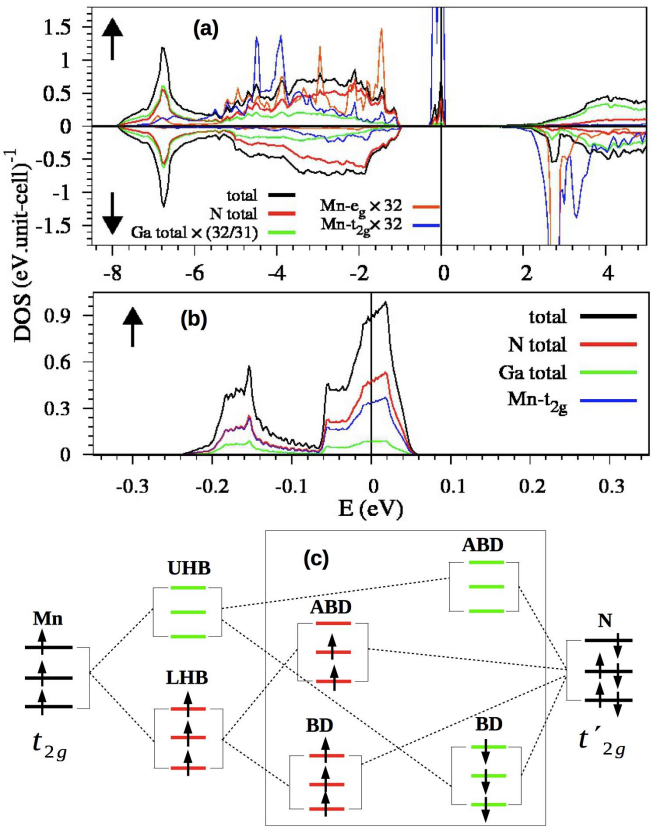

FIG. 1. (color online) (a) Total and partial densities of states (DOS) of $Ga_{31}MnN_{32}$ with the Fermi energy (E_F) at 0 eV. The partial DOSs have been scaled up in units of "per atom of this kind". (b) The DOS of the impurity bands around E_F in units of "per GaN primitive unitcell". (c) Illustration of the hybridization of Mn-N orbitals. Up and down arrows represent spin majority and minority, respectively. UHB (LHB) denotes upper (lower) Hubbard bands, whereas BD (ABD) denotes bonding (anti-bonding). Note that two electrons residing in the spin-majority e_g orbitals are not shown here.

1(a) shows clearly that part of the 5.0 d electrons resides in the spin minority channel spreading over a large energy range, as a consequence of the strong hybridization with the N orbitals. A simpler visualization of this beyond-ionic configuration is given by Fig. 1(c) that summarizes the basic building blocks of the electronic structure. It is now clear that the Mn ion hosts part of a hole in the anti-bonding orbitals of the lower Hubbard bands (LHB), and part of three electrons in the bonding orbitals of the upper Hubbard bands (UHB). Specifically, we found 0.5 electrons in the Mn spin-minority channel, and 4.5 in the majority one, giving a net moment of 4.0 μ_B. (The N orbitals that hybridize with Mn orbitals, named N-t'_{2g} in Fig. 1(c), will be defined in detailed below.)

Obviously now, the strong hybridization between Mn and N orbitals renders the high-energy ionic picture based on atomic orbitals completely inapplicable in the lower-energy sector, in which the renormalized orbitals

absorb the hybridization upon integrating-out the higher-energy degrees of freedom. In other words, at low energy, electrons are no longer able to reside in Mn or N atomic orbitals, but only in Mn-N hybrids. Therefore, debating the ionic valency with atomic orbitals is of no physical significance for the low-energy behavior of the system. Instead, the physics should be described by effective or "renormalized" Mn and N orbitals.

Interestingly, the proximity of the N and Mn orbital energies, which enhances the hybridization and other quantum effects, also enables the generic possibility of multiple representations of the many-body system. It is feasible to derive multiple low-energy effective pictures, depending on which is more convenient for describing the physical properties of interest. Below, we demonstrate this fundamental feature by constructing various low-energy effective WOs that corresponds to integrating-out higher-energy degrees of freedom differently. Specifically, we show that both effective d^4 and d^5 pictures can be derived, and both are useful for describing certain properties.

We start with the local properties of $Ga_{1-x}Mn_xN$. Fig. 1(b) shows a $\frac{2}{3}$–filled impurity level, corresponding to two electrons residing in three degenerate "effective" t_{2g} WOs. One thus expects a strong local Jahn-Teller instability toward splitting the degeneracy into $2+1$. Indeed, the Jahn-Teller instability has been found in previous studies [55, 56]. It is easier to describe this local physics using an "effective" d^4 picture. Fig. 2 (a) shows one of the "effective" $\widetilde{\text{Mn}}$-t_{2g} WOs corresponding to the impurity levels between [-0.4,0.4]. It has the symmetry of the Mn-t_{2g} orbital, but with large tails in the surrounding N ions, incorporating the anti-bonding hybridization illustrated in Fig. 1(c). It is in this "effective" $\widetilde{\text{Mn}}$-t_{2g} WOs that an effective d^4 picture is realized: A three-fold degenerate WOs hosting two electrons, which then split into $2+1$ orbitals upon orbital polarization. (The other two electrons reside in the spin-majority effective e_g WOs.) This effective d^4 picture also gives a local moment of $4\mu_B$ that is really the one fluctuating at low-energy, with a form factor [57, 58] extending to neighboring N ions in real-space.

An interesting point that emerges here is that the hybridization with Mn-t_{2g} naturally splits the surrounding four N-sp^3 orbitals, one from each N ion pointing toward Mn, into a set of $3+1$ configurations. The three-fold degenerate ones have the correct signs to match each of the Mn-t_{2g} orbitals: (+,+,-,-), (+,-,+,-), (+,-,-,+), while the fourth one with sign (+,+,+,+) does not couple to the Mn-t_{2g} orbitals. One thus can conveniently name them N-t'_{2g} and N-s' WOs centered at the Mn site. The four tails of the WOs in Fig. 2 (a) give an example of one of these N-t'_{2g} orbitals which in Fig. 1(c) hybridize with Mn-t_{2g}. These N-t'_{2g} are the ones being integrated out to derive the effective d^4 picture. Note that this change of perspective is the same as that employed in the construction of the well-known Zhang-Rice singlet in the cuprate high-temperature superconductors [59, 60], and the same concept has been applied to the study of local excitations in correlated NiO [58, 61] and LiF [62, 63].

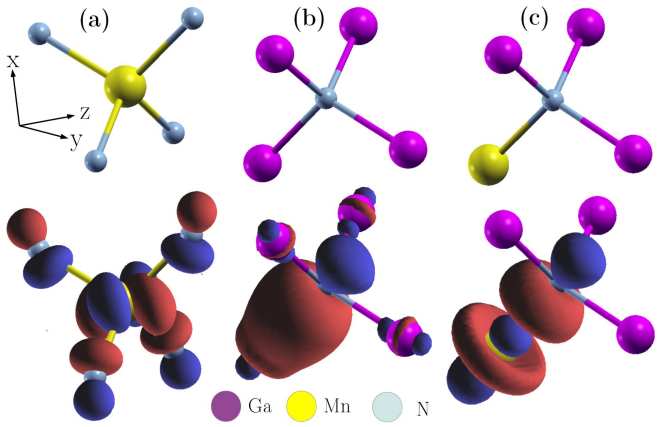

FIG. 2. (color online) Illustration of the WOs used in (a) low-energy effective d^4 and (b)-(c) effective d^5 picture. The upper panels show the local crystal structure, while the lower panels plot the iso-surface of (a) $\widetilde{\text{Mn}}-t_{2g}$, and (b)(c) $\widetilde{\text{N}}-sp^3$ WOs at 0.07 bohr$^{-3/2}$.

The above effective d^4 picture, while ideal to study the Jahn-Teller instability and other local properties like the local magnetic moment and local excitations, is not suitable for studying long-range properties. This is because the wave nature of the GaN orbitals, after being integrated out, generates effective magnetic couplings that are impurity-configuration dependent between the $\widetilde{\text{Mn}}$ WOs at different sites. For instance, the magnetic coupling does not only depend on the distance between pairs of Mn impurities [24], but also on the position of other nearby Mn impurities, corresponding to three-body and four-body interactions [64].

Therefore, we proceed to derive an effective d^5 picture suitable for studying long-range properties, by integrating out charge fluctuation involving Mn-d and Ga orbitals in the multi-orbital Anderson Hamiltonian, leaving only the doped hole in the anti-bonding WOs with primarily N-sp^3 character. From this we obtain a spin-fermion Hamiltonian with a few novel physical effects: $H_{\text{eff}} = H_0 + \Delta$, where

$$H_0 = \sum_{\mathbf{ii'}mm'\sigma} t^{mm'}_{\mathbf{ii'}} c^\dagger_{\mathbf{i}m\sigma} c_{\mathbf{i'}m'\sigma} + \ h.c. \tag{1}$$

is the Hamiltonian of pure GaN, and

$$\Delta = \sum_{\mathbf{jii'}mm'\sigma} T^{mm'}_{\mathbf{jii'}} c^\dagger_{\mathbf{i}m\sigma} c_{\mathbf{i'}m'\sigma} + \sum_{\substack{\mathbf{jii'}mm'\\ \sigma\sigma'}} J^{mm'}_{\mathbf{jii'}} c^\dagger_{\mathbf{i}m\sigma} \boldsymbol{\tau}_{\sigma\sigma'} c_{\mathbf{i'}m'\sigma'} \cdot \hat{\boldsymbol{S}}_{\mathbf{j}} \ + \ h.c. \tag{2}$$

contains the influence of the (Ga,Mn) substitution at the primitive unit-cell $\mathbf{j}$, and is thus referred to as impurity potential. As usual, $c_{\mathbf{i}m\sigma}$ ($c^{\dagger}_{\mathbf{i}m\sigma}$) annihilates (creates) an electron with spin σ at unit-cell $\mathbf{i}$ in the m-th WOs. $t^{mm'}_{\mathbf{ii'}}$ contains the orbital energy (when $\mathbf{i} = \mathbf{i'}$ and $m = m'$) and hopping integral of the "effective" $\widetilde{\text{N}}$-sp^3 WOs. $T^{mm'}_{\mathbf{jii'}}$ and $J^{mm'}_{\mathbf{jii'}}$ represent spin-independent and spin-dependent impurity potentials, respectively. $\hat{\boldsymbol{S}}_{\mathbf{j}}$ and $\boldsymbol{\tau}_{\sigma\sigma'}$ are the spin-$\frac{5}{2}$ unit-vector and elements of the Pauli's matrices, respectively, and *h.c.* denotes the Hermitian conjugate. To get a better understanding on the origin of this generalized spin-fermion model we illustrate the derivation of the impurity potentials from perturbation theory using a simple model in the Supplemental Material [65].

Note that the four WOs with the same unit-cell index are defined to be the $\widetilde{\text{N}}$-sp^3 WOs pointing toward the central Ga/Mn ion, one from each surrounding N ion. With the help of symmetry considerations [65] we choose the proper WOs subspace corresponding to integrating out the Mn and Ga orbitals. These WOs can be constructed from our DFT results within the energy range $[-18.0,\ 0.4]$ eV, as shown in Fig. 2 (b)-(c). In their hybridization tails, one observes clearly bonding with Ga-sp^3 [Fig. 2(b)] and anti-bonding with Mn-d [Fig. 2(c)].

Having these WOs at hand, we can then represent the relevant part of the DFT self-consistent Hamiltonian and collect its term into the form of Eqs. (1) and (2). Since this is a faithful representation of the relevant components of the DFT Hamiltonian, its validity is actually beyond the 2$^{\text{nd}}$ order in the atomic hopping integral. A few leading parameters in our results are given in Table I. As expected, they show a rapid decay with the distance from the impurity site.

TABLE I. Leading parameters in the impurity potential in meV near the impurity site $\mathbf{j}$. NN($\mathbf{j}$) and NNN($\mathbf{j}$) denotes nearest neighboring and next nearest neighboring sites. Here, $m \neq m'$.

	$T^{mm}_{\mathbf{jji'}}$	$T^{mm'}_{\mathbf{jji'}}$	$J^{mm}_{\mathbf{jji'}}$	$J^{mm'}_{\mathbf{jji'}}$
$\mathbf{i'} = \mathbf{j}$	2488	−170	1752	−633
$\mathbf{i'} = \text{NN}(\mathbf{j})$	406	885	449	800
$\mathbf{i'} = \text{NNN}(\mathbf{j})$	15	68	< 10	38

Interestingly, our results reveal a few new physical effects on the carriers besides the previously proposed [25] anti-ferromagnetic exchange with the local moment ($J^{mm}_{\mathbf{jjj}} = 1752$ meV in Tab. I). First, the impurity potential contains a strong shift of the orbital energy ($T^{mm}_{\mathbf{jjj}} = 2488$ meV), even *stronger* than the exchange above. This reflects the distinct atomic orbitals of Mn (the impurity) and Ga (the host) being integrated out. In fact, our test shows that if one were to ignore just this parameter, the impurity level [red bands in Fig. 3(a)] would have dropped outside the band gap [c.f. Fig. 3(b)], totally destroying the physical characteristics of the system. Physically, this large orbital energy shift of course induces a strong impurity scattering and a strong tendency toward Anderson localization [66], affecting the carrier mobility, the activation energy, and almost every other essential physical aspects of a semiconductor, in addition to altering the effective magnetic coupling between Mn ions. Second, our results also show a strong exchange-assisted hopping ($J^{m\neq m'}_{\mathbf{jji'}} = -633$ meV and 800 meV in Tabel I close to the impurity site.) Again, Fig. 3(c) shows that ignoring these two terms lead to a much smaller spin-dependent splitting of the impurity level. Therefore, they not only add to the above impurity effects but also directly modify the magnetic exchange and ordering of Mn impurities. Both of these two effects are very strong and comparable in strength to the exchange effect included in previous studies, and thus will need to be further investigated in the future.

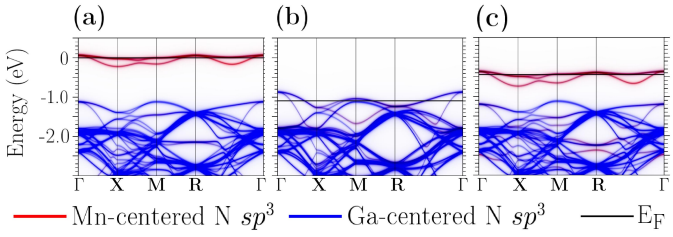

FIG. 3. (color online) The spin-majority band structure of $Ga_{31}MnN_{32}$ (a) with complete parameters, (b) with the leading orbital energy shift $T^{mm}_{\mathbf{jjj}} = 2488$ meV removed, and (c) with the two leading exchange-assisted parameters $J^{mm'\neq m}_{\mathbf{jjj}} = -633$ and $J^{mm'\neq m}_{\mathbf{jji'}} = 800$ meV with $\mathbf{i'} = \text{NN}(\mathbf{j})$ removed.

It is useful to remark that our approach of employing multiple pictures in understanding different low-energy properties of a many-body system have been used in other strongly correlated materials, for examples, in the manganites and the cuprates. Specifically for the cuprates, the Zhang-Rice singlet description [59] and Emery-Reiter three-spin polaron description [67] are exactly effective d^8 and d^9 pictures, parallel to our d^4 and d^5. The d^8 approach integrates the oxygen degrees of freedom out, resulting in a reduced local magnetic moment $S = 0$, similar to our effective d^4 picture that absorbs implicitly the GaN orbitals and has a smaller moment $S = 2$. On the other hand, the d^9 picture integrates charge fluctuation involving the Cu orbitals out and results on doped holes propagating in O orbitals that are correlated anti-ferromagnetically with the surrounding Cu $S = 1/2$ spins, similar to our effective d^5 picture in which carriers live in effective $\widetilde{\text{N}}$-sp^3 WOs that correlated anti-ferromagnetically with the Mn $S = 5/2$ spins. Naturally, the more complete d^9 picture of cuprates and our d^5 picture of (Ga,Mn)N cover a larger energy range

than the d^8 and d^4 picture respectively, and thus allow richer physical behaviors in general.

To summarize, by investigating the current debate on the Mn valence in $Ga_{1-x}Mn_xN$, we advocate three general points in correlated materials: 1) atomic or ionic valence is only meaningful for high-energy properties but is not very relevant to the low-energy physical properties; 2) it is often possible to derive multiple effective pictures by integrating out the less relevant degrees of freedom; and 3) for challenging correlated systems, one thus should take advantage of such flexibility and employ the most convenient picture for describing the physical properties of interest. Specifically, we found the Mn valence of 2+, but with a non-atomic spin of $4\mu_B$; illustrating the inadequacy of ionic valence in an atomic picture. We then demonstrate the feasibility of an effective d^4 picture (naturally with $S = 4$) suitable for studying local instabilities and excitations. In addition, we derive an effective d^5 approach that can be used for future studies of long-range magnetic order, non-local magnetic correlation, and other transport properties. Particularly, our d^5 model demonstrates a few novel physical effects beyond previous considerations in the field. Our results clarify the intrinsic dual nature of the doped holes in the DMS and pave the way for future realistic studies of the magnetism in these systems. Our study not only resolves one of the outstanding key puzzles in the field, but also emphasizes the general need for multiple effective pictures to describe the rich low-energy physics in many-body systems in general.

We thank P. Derosa for useful feedback on our manuscript. This work is supported by NSF DMR-1237565 and NSF EPSCoR Cooperative Agreement No. EPS-1003897 with additional support from the Louisiana Board of Regents. WK and TB were supported by DOE CMCSN DE-AC02-98CH10886. TB also acknowledges additional support from the Wigner Fellowship of Oak Ridge National Laboratory. Work by T. B. was partly performed at the Center for Nanophase Materials Sciences, a DOE Office of Science user facility. Supercomputer support is provided by the Louisiana Optical Network Initiative (LONI) and HPC@LSU computing resources.

[1] I. Žutić, J. Fabian, and S. D. Sarma, Rev. Mod. Phys. **76**, 323 (2004).
[2] G. A. Prinz, Science **282**, 1660/1 (1998).
[3] S. D. Sarma, Am. Scientist **89**, 516 (2001).
[4] I. Žutić, J. Fabian, and S. Das Sarma, Appl. Phys. Lett. **79**, 1558 (2001).
[5] B. Endres *et al.*, Nature Commun. **4**, 2068 (2013).
[6] Y. Ohno *et al.*, Nature **402**, 790 (1999).
[7] S. A. Wolf *et al.*, Science **294**, 1488 (2001).
[8] S. J. Pearton *et al.*, J. Phys.: Condens. Matter **16**, R209 (2004).
[9] H. Amano *et al.*, Appl. Phys. Lett. **48**, 353 (1986).
[10] I. Akasaki *et al.*, J. of Crystal Growth **128**, 379 (1993).
[11] S. Nakamura, T. Mukai, and M. Senoh, Appl. Phys. Lett. **64**, 1687 (1994).
[12] T. Dietl, H. Ohno, and F. Matsukura, Phys. Rev. B **63**, 195205 (2001).
[13] D. Chen *et al.*, Nucl. Inst. and Meth. in Phys. Res. B **266**, 2797 (2008).
[14] M. Zając *et al.*, Appl. Phys. Lett. **79**, 2432 (2001).
[15] S. Granville *et al.*, Phys. Rev. B **81**, 184425 (2010).
[16] S. Dhar *et al.*, Phys. Rev. B **67**, 165205 (2003).
[17] M. E. Overberg *et al.*, Appl. Phys. Lett. **79**, 1312 (2001).
[18] S. Stefanowicz *et al.*, Phys. Rev. B **88**, 081201(R) (2013).
[19] G. T. Thaler *et al.*, Appl. Phys. Lett. **80**, 3964 (2002).
[20] M. L. Reed *et al.*, Appl. Phys. Lett. **79**, 3473 (2001).
[21] T. Sasaki *et al.*, J. Appl. Phys. **91**, 7911 (2002).
[22] T. Jungwirth, J. Sinova, J. Mašek, J. Kučera, and A. H. MacDonald, Rev. Mod. Phys. **78**, 809 (2006).
[23] C. Liu, F. Yun, and H. Morko, J. Mater. Sci.: Mater. Electron. **16**, 555 (2005).
[24] K. Sato *et al.*, Rev. Mod. Phys. **82**, 1633 (2010).
[25] M. Abolfath, T. Jungwirth, J. Brum, and A. H. MacDonald, Phys. Rev. B **63**, 054418 (2001).
[26] C. Zener, Phys. Rev. **81**, 440 (1951).
[27] T. Hayashi, Y. Hashimoto, S. Katsumoto, and Y. Iye, Appl. Phys. Lett. **78**, 1691 (2001).
[28] K. W. Edmonds *et al.*, Appl. Phys. Lett. **81**, 4991 (2002).
[29] K. M. Yu *et al.*, Phys. Rev. B **65**, 201303(R) (2002).
[30] L. P. Rokhinson *et al.*, PRB **76**, 161201(R) (2007).
[31] C. Zener, Phys. Rev. **82**, 403 (1951).
[32] N. Furukawa, in *Physics of Manganites*, edited by Kaplan and Mahanti (Plenum, 1999) pp. 1–38.
[33] K. Sato *et al.*, J. Phys.: Condens. Matter **16**, S5491 (2004).
[34] R. Y. Korotkov, J. M. Gregie, and B. W. Wessels, Physica B **308**, 30 (2001).
[35] R. Y. Korotkov, J. M. Gregie, and B. W. Wessels, Appl. Phys. Lett. **80**, 1731 (2002).
[36] K. S. Burch *et al.*, J. Magn. Magn. Mater. **320**, 3207 (2008).
[37] E. Kulatov, H. Nakayama, H. Mariette, H. Ohta, and Y. A. Uspenskii, Phys. Rev. B **66**, 045203 (2002).
[38] B. Sanyal, O. Bengone, and S. Mirbt, Phys. Rev. B **68**, 205210 (2003).
[39] L. M. Sandratskii, P. Bruno, and J. Kudrnovský, Phys. Rev. B **69**, 195203 (2004).
[40] M. Wierzbowska *et al.*, Phys. Rev. B **70**, 235209 (2004).
[41] J. Kang, K. J. Chang, and H. Katayama-Yoshida, J. Supercond.: Incorporating Novel Magnetism **18**, 55 (2005).
[42] P. Mahadevan and A. Zunger, Phys. Rev. B **69**, 115211 (2004).
[43] J. Schneider *et al.*, Phys. Rev. Lett. **59**, 240 (1987).
[44] X. Biquard *et al.*, J. Supercond.: Incorporating Novel Magnetism **16**, 127 (2003).
[45] A. Titov *et al.*, Phys. Rev. B **72**, 115209 (2005).
[46] W. Stefanowicz *et al.*, Phys. Rev. B **81**, 235210 (2010).
[47] T. Graf *et al.*, Appl. Phys. Lett. **81**, 5159 (2002).
[48] T. Graf *et al.*, J. Appl. Phys. **93**, 9697 (2003).
[49] Y. L. Soo *et al.*, Appl. Phys. Lett. **79**, 3926 (2001).
[50] K. W. Edmonds *et al.*, J. Appl. Phys. **95**, 7166 (2004).
[51] J. I. Hwang *et al.*, Phys. Rev. B **72**, 085216 (2005).
[52] W. Ku *et al.*, Phys. Rev. Lett. **89**, 167204 (2002).
[53] P. Blaha, K. Schwarz, G. Madsen, D. Kvasnicka, and

J. Luitz, "Wien2k, an augmented plane wave+local orbitals program for calculating crystal structure," (K. Schwarz Technical University, Wien, Austria, 2001).
[54] V. I. Anisimov *et al.*, Phys. Rev. B **48**, 16929 (1993).
[55] X. Luo and R. M. Martin, Phys. Rev. B **72**, 035212 (2005).
[56] A. Boukortt *et al.*, Phys. Rev. B **85**, 033302 (2012).
[57] A. C. Walters *et al.*, Nat. Phys. **5**, 867 (2010).
[58] B. C. Larson *et al.*, Phys. Rev. Lett. **99**, 026401 (2007).
[59] F. C. Zhang and T. M. Rice, Phys. Rev. B **37**, 3759 (1988).
[60] W.-G. Yin and W. Ku, Phys. Rev. B **79**, 214512(R) (2009).
[61] C.-C. Lee *et al.*, Phys. Rev. B **82**, 081106(R) (2010).
[62] C.-C. Lee *et al.*, Phys. Rev. Lett. **111**, 157401 (2013).
[63] P. Abbamonte *et al.*, PNAS **105**, 12159 (2008).
[64] X. Y. Cui, B. Delley, A. J. Freeman, and C. Stampfl, Phys. Rev. B **76**, 045201 (2007).
[65] See Supplemental Material at ... for the details of the derivation.
[66] P. W. Anderson, Physical Review **109**, 1492 (1958).
[67] V. J. Emery and G. Reiter, Phys. Rev. B **38**, 4547 (1988).